International Journal of Database Theory and Application
Vol.7, No.3 (2014), pp.159-178
http://dx.doi.org/10.14257/ijdta.2014.7.3.15

An Investigation into the Impact of False Minutiae Points on Fingerprint Matching

Iwasokun Gabriel Babatunde, Akinyokun Oluwole Charles and Ojo Sunday Olusegun

Tshwane University of Technology, Pretoria, South Africa
Federal University of Technology, Akure, Nigeria
IwasokunGB@tut.ac.za, akinwole2003@yahoo.co.uk, OjoSO@tut.ac.za

Abstract

This paper presents a report on the experimental study of the impact of false minutiae on the performance of fingerprint matching systems. A 3-tier algorithm comprising of pre-processing, minutiae extraction and post-processing stages formed the backbone of the experiments. The pre-processing stage enhanced the fingerprint image, the minutiae extraction stage used the minutiae properties to detect and extract true and false minutiae points while the post-processing stage eliminated the false minutiae points. The experiments were performed on the four datasets in each of the three standard fingerprint databases; namely FVC2000, FVC2002 and FVC2004. The completion times for the minutiae extraction and the post-processing algorithms on each dataset were measured. A standard fingerprint matching algorithm was also implemented for verifying the impact of false minutiae points on FAR, FRR and the matching speed. Analysis of the obtained results revealed that for reliable and optimal performance of fingerprint matching systems, false minutiae points must be eliminated as much as possible from their operations.

Keywords: *AFIS, experimental study, fingerprint, minutiae point, fingerprint databases, fingerprint matching*

1. Introduction

Automated Fingerprint Identification System (AFIS) is a device for human verification and identification in places or centers where human traffic management and control are required [1-3]. The recent upsurge in the acceptance and use of AFIS over the other biometrics-based devices has been attributed to a number of factors which include:

a. Fingerprint exhibits properties that are highly unique from individual to individual

b. It is possessed by every individual

c. It maintains durable and consistent form in one's lifetime

d. There are wide range of low-cost devices and technologies for fingerprint enrolment and processing

The steps involved in the operation of most AFISs are conceptualized in Figure 1. For consistent and reliable performance, trust worthy matching or rejection results must be obtained. Very low False Acceptance Rate (FAR) and False Rejection Rate (FRR) are also expected for users' acceptability and patronage. To achieve these objectives, suitable and reliable algorithms must form the backbone of these steps.

ISSN: 2005-4270 IJDTA
Copyright ⓒ 2014 SERSC

Sequel to fingerprint image enrolment, several enhancement activities including pre-processing, segmentation, normalization and image filtering are performed. Local variance and angular definitions constitute the method for fingerprint segmentation to separate the fingerprint foreground from its background. Normalization is also performed for standardization of the ridge grey level values [4]. Several methods including Gabor filter [5-10], Short Time Fourier Transform [11] and Directional Filter [12-14] are some of the most popular approach to filtering fingerprint ridge and valley patterns in gray levels. At the fingerprint enhancement stage, all the noises and the contaminants introduced during enrolment are removed to pave way for smooth and accurate minutiae extraction. The extracted minutiae then formed the reference minutiae set that is matched with pre-created minutiae sets in the template database. Commonly used minutiae are the end points (enclosed in circles) and bifurcations (enclosed in square) in Figure 2 [15-19]. The ridge terminates at the end point while it splits into two at the bifurcation point.

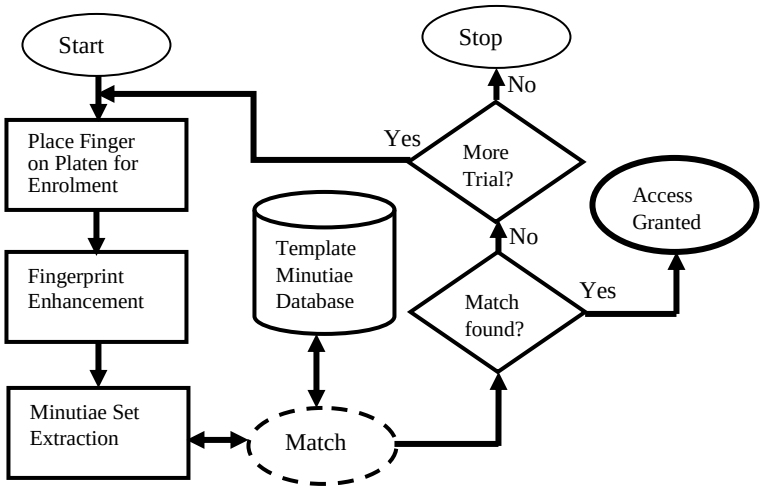

Figure 1. Operational Steps of AFIS

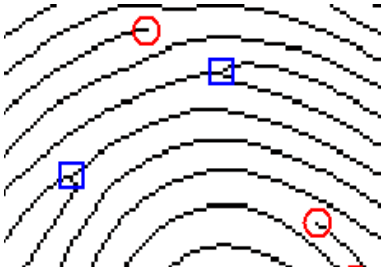

Figure 2. Fingerprint Ridges Showing End and Bifurcation Points

Based on specified algorithm, the characteristics (orientation, coordinate and distance relative to singular point) for the minutiae set of an image is compared (matched) with those for other images to establish or reject claim of identity. The implementation of very safe and reliable fingerprint minutiae extraction strategies is therefore important for ensuring accuracy [16-18]. Existing research works on fingerprint minutiae extraction include the use of Adaptive Flow Orientation [19-20], Mathematical Morphology [21-22]; Ridge Tracing [23-

 Copyright ⓒ 2014 SERSC

24], Fuzzy Image [25] and Complex filtering [26-27]. Others are Weighted Audio Spectrum Flatness-WASF [28], Stochasitic Resonance [29], Cellular Neural Networks [30] and Pseudo Zernike Moments [31]. Section 2 of this paper presents the review of some existing works while Section 4 discusses the fingerprint minutiae extraction technique. Sections 4 and 5 present the experimental study and the conclusion drawn respectively.

2. Some Existing Works

Several techniques have emerged for fingerprint minutiae extraction with their respective strengths and weaknesses. The authors in [29] presented a stochastic resonance approach for feature extraction from low-quality fingerprints. Gaussian noise was added to the original fingerprint images earlier rejected due to low-quality by some state-of-the-art fingerprint verification algorithms before extraction. Though, the approach failed with fingerprints with no meaningful features, obtained results showed significant improvement in the equal error and genuine acceptance rates. The authors in [23] presented an algorithm for minutiae extraction from skeletonized and binarized images. An algorithm was also proposed for ridge cleansing based on ridge positions and directional maps. The obtained results showed efficient reduction of spurious minutiae with good performances in dirty areas but the algorithm experiences low processing speed due to computational complexity. The authors in [24] proposed an algorithm for the extraction of fingerprint features from gray scale images by ridge tracing which used contextual information to handle noisy regions with used parameters made adaptive for circumventing human supervision. The algorithm is suitable for speedy extraction of minutiae points but susceptible to extraction of type-exchange minutiae as well as dropped features like short ridges and spurs. Mathematical morphology algorithm is used in [21-22] to remove the superfluous information for genuine feature extraction and measure performance through sensitivity and specificity. The algorithm effectively removed spurious structures and extracted clear and reliable ridge map from input fingerprint image but experienced a number of missed genuine minutiae.

A set of local feature descriptors for fingerprints is proposed in [26]. Minutiae points are detected through a complex filtering of the structure tensor by revealing their positions and directions. Model formulation was by parabolic and linear symmetry descriptions for the extraction of local features and their ridge orientations and reliabilities. Although results on their application in several stages of fingerprint recognition systems showed efficiency, the descriptors failed with severely distorted images. The authors in [30] proposed Cellular Neural Networks (CNN) algorithm for the extraction of high percentage of genuine feature points and their corresponding direction attributes from thinned fingerprint images. The algorithm rejects spurious feature points resulting from noisy fingerprints, but show low computational speed due to un-optimized procedures. A fingerprint local invariant feature extraction using Feature Transform (SIFT) and Speeded-Up Robust Feature (SURF) detectors is proposed in [32].The detectors run on the central and graphic processing units and focus on the consumed time as important factor for fingerprint identification. The implementations produced promising behaviors for the two detectors with very short processing time.

A method for direct extraction of features from gray-level fingerprint images without binarization and thinning is proposed in [33]. The algorithm traced the ridges, recorded the skeleton image and acquired minutiae with robustness and efficiency. The authors in [15, 17] used Crossing Numbers (CN) algorithms that is based on ridge scanning for fingerprint minutiae extraction. For bad quality image, the algorithm is prone to extraction of exceeding number of false minutiae prompting the authors in [15] to use a post-processing stage to eliminate all forms of spurious features using their ridge and neighborhood characteristics. A

Copyright ⓒ 2014 SERSC

features detection method which reduces the likelihood of an unreliable overlapping region in partial fingerprint is proposed in [34]. The method provides significant improvement for matching low quality images but fails with too much overlapping areas.

A Gabor filter-based method for direct extraction of fingerprint minutiae from grey-level images without pre-processing is proposed in [35]. The method demonstrated efficiency and suitability than other conventional methods but failed with images whose grey-level cannot be determined. The algorithm solved some fingerprint recognition problems relating to translation, scaling and rotation. The authors in [25, 36] implemented algorithms for high level minutiae extraction for all fingerprint images based on pre-processing stages (singular point detection, orientation field estimation and Gabor filter). The performance of these algorithms however depends on the precision of directional and frequency maps. The authors in [31] presented invariant fingerprint minutiae extraction algorithm based on Pseudo Zernike Moments [37-38] and Bayesian classifier [39].

3. Fingerprint Minutiae Extraction Technique

The algorithm that formed the basis of minutiae extraction experiments is conceptualized in Figure 3 showing the pre-processing, minutiae extraction and validation stages.

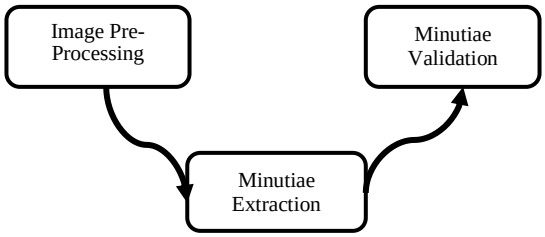

Figure 3. Fingerprint Filtering Stages

3.1. Image Pre-Processing

For smooth and reliable minutiae extraction, the enrolled fingerprint image is taken through a pre-processing stage of enhancement. The stage includes segmentation, normalization, ridge orientation and frequency estimation, filtering, binarization and thinning. The essence of segmentation is to clearly divide the background region from the foreground region. The background regions generally exhibit high noise and contaminant levels as well as very low grey-scale variance values. On the contrary the foreground regions possess very high variances with minimal noise and contaminants. Based on these characteristics, variance thresholding technique is used to separate the background from the foreground regions. The first step is to divide the image into blocks followed by the calculation of the grey-scale variance for each block. A block with variance exceeding the global threshold is assigned to the foreground otherwise it is assigned to the foreground. The grey-level variance for a block, b with size β *x* β is defined as [4, 40]:

$$\sigma(b) = \sigma^{-2} \sum_{m=0}^{\beta-1} \sum_{n=0}^{\beta-1} V \quad (1)$$

$$V = (B(m,n) - \mu(b))^2 \quad (2)$$

$\sigma(b)$ is the variance for block b, $B(m,n)$ is the grey-level value at pixel (m,n), and $\mu(b)$ is the mean grey-level value for the block b.

 Copyright ⓒ 2014 SERSC

The segmented image is normalised by regulating its grey-level values to attain uniformity and fall within desired range. If $\rho(r,s)$ represents the grey-level value at pixel (*r*,*s*), and $\beta(r,s)$ represents the normalised grey-level value at pixel (*r*,*s*), the normalized image is derived from:

$$\beta(r,s) = \begin{cases} \gamma_0 + \sqrt{(\vartheta_0(\rho(r,s)-\gamma)^2)\vartheta^{-1}} & if\ \ \rho(r,s) > \gamma \\ \gamma_0 - \sqrt{(\vartheta_0(\rho(r,s)-\gamma)^2)\vartheta^{-1}} & otherwise \end{cases} \quad (3)$$

γ and ϑ are the calculated mean and variance of $\rho(r,s)$, respectively while γ_0 and ϑ_0 are the desired mean and variance respectively.

The orientation field of a fingerprint image gives the local orientation of its ridges. It is computed by dividing the image into blocks of uniform sizes and the local orientation for a block with centre at pixel (r,s) is computed from [40-42]:

$$V_x(r,s) = \sum_{p=r-\frac{W}{2}}^{r+\frac{W}{2}} \sum_{q=s-\frac{W}{2}}^{s+\frac{W}{2}} 2\partial_x(p,q)\partial_y(p,q) \quad (4)$$

$$V_y(r,s) = \sum_{p=r-\frac{W}{2}}^{r+\frac{W}{2}} \sum_{q=s-\frac{W}{2}}^{s+\frac{W}{2}} \partial_x^2(p,q) - \partial_y^2(p,q) \quad (5)$$

$$\theta(r,s) = \frac{1}{2}\tan^{-1}\frac{V_y(r,s)}{V_x(r,s)} \quad (6)$$

∂_x(p,q) and ∂_y(p,q) are the gradients obtained using any gradient operator at point (p,q) in x and y directions respectively. Θ(r,s) is the least square estimate of the local orientation of the block with centre at pixel (r,s).

The ridge frequency estimation algorithm produces a coarse-level ridge map of the input fingerprint image and it is based on pre-estimated local ridge orientations. Grey levels along fingerprint ridges and valleys are modeled as sinusoidal shaped wave along the normal direction to the local orientation. The wave is principally utilized for the estimation of the ridge frequency based on the assumptions that valid ridge frequencies lie between 1/31 and 1/25 for 500dpi images [6, 43-44]. Fingerprint image filtering is based on the periodic function G(x, y; f, ɵ) as follows [8].

$$\mathrm{G(x,y:f,\theta)} = \exp\left[0.5\left[\frac{\alpha^2\vartheta_y^2 + \beta^2\vartheta_x^2}{\vartheta_x^2\vartheta_y^2}\right]\right]\cos(2\pi f\alpha) \quad (7)$$

$$\alpha = xsin\theta + ycos\theta \quad (8)$$

$$\beta = xcos\theta + ysin\theta \quad (9)$$

f represents the frequency of the sinusoidal plane wave along the direction θ from the *x*-axis, and ϑ_x and ϑ_y are the space constants empirically determined and set to about half the average inter-ridge distance in their respective direction. The filtered image is binarized using the method proposed in [45] to obtain its best performance threshold. The threshold (T) is set for making each cluster as tight as possible, thereby minimizing their overlap. T is determined by separating the pixels into two clusters based on presumed thresholds and the mean of each

Copyright ⓒ 2014 SERSC

cluster is determined. The difference between the means is squared and the product of the number of pixels in one cluster and the number in the other is determined. The success of these operations is determined by the difference between the means of the clusters while the optimal threshold maximizes the between-class variance or minimizes the within-class variance. The binarized image is thinned with the Matlab '*bwmorph'* operation using the '*thin*' option to generate the thin or skeleton image.

3.2. Minutiae Extraction

During minutiae extraction, a fingerprint image is viewed as a flow pattern with a definite texture from which an orientation field for the flow texture is computed [46]. From a filtered (thinned) image, a minutia point is extracted based on its CN value obtained from:

$$CN = \sum_{i=0}^{7} |N_{i+2} - N_{i+1}|, \qquad N_9 = N_1 \tag{10}$$

N_1, N_2, …, N_8 represent the 8 neighbours of the candidate minutia point N, in its 3 x 3 neighbourhood which are scanned in the direction shown in Figure 4.

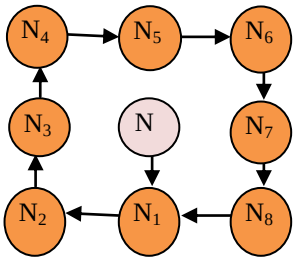

Figure 4. 8 Neighbors of a Candidate Minutiae Point

Table 1 shows the existing CN properties of 2 and 6 denoting ridge end and bifurcation points respectively. The isolated, continuous and crossing points produced spur, hole, triangle and spike structures which are all regarded as false minutiae points. As shown in Figure 5, the spur structure generates false ridge endings while the hole and triangle structures produce false bifurcations. The spike structure also creates a false bifurcation and a false ridge ending point [15, 41, 47]. Figure 6 shows candidate ridge pixels (at the centre of the enclosed ridges) for ridge ending and bifurcation points.

Table 1. CN Number and its Property

S/No.	CN	Property
1	0	Isolated point
2	2	Ridge ending point
3	4	Continuous ridge point
4	6	Bifurcation point
5	8	Crossing point

Copyright ⓒ 2014 SERSC

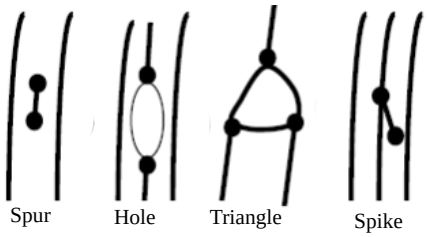

Figure 5. False Minutiae Structures

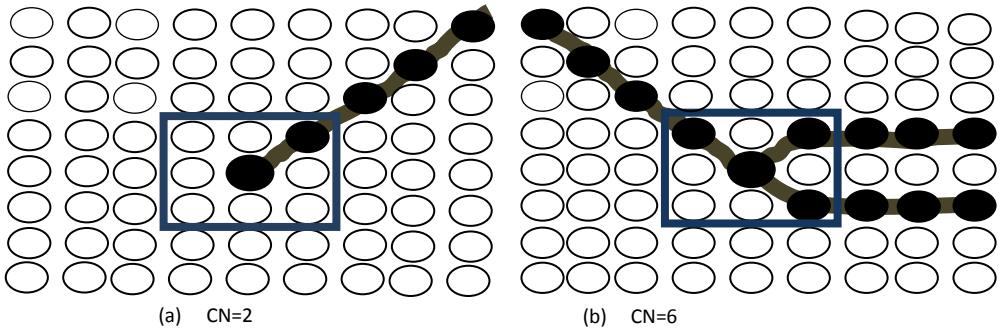

Figure 6. CN Values for Ridge Ending and Bifurcation Points

3.3. Post-Processing

For the elimination of all the false minutiae points, a post-processing algorithm [15, 20, 40] is implemented. The algorithm firstly creates an image M of size W x W and centred on the candidate minutia point. The validity of the candidate point is then tested by examining the properties of its 3 x 3 neighbourhood. This involves labelling the centre pixel with -1 while the connected pixels are initialized to zero, as shown in Figure 7(a) and Figure 7(c) for candidate ridge ending and bifurcation points respectively.

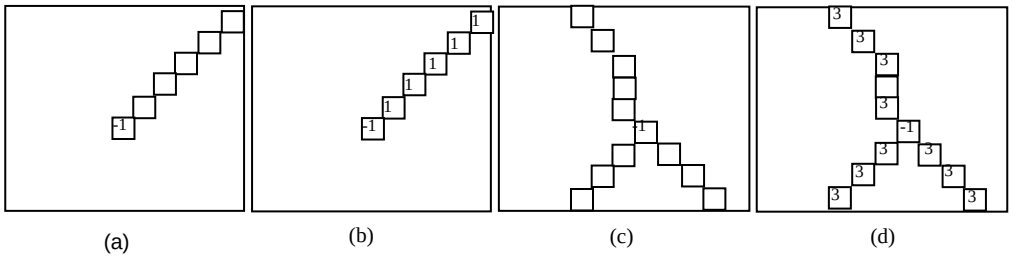

Figure 7. Labelling and Initialization of Candidate Minutiae Points and its Connected Pixels

Then for every ridge ending candidate point, all the connecting pixels are initialized to 1 (Figure 7(b)) and the number of 0 to 1 transitions in clockwise direction (T01) along the border of M is determined. If T01 = 1 (Figure 8(a)), then the candidate minutia point is a true ridge ending. Similarly, for each bifurcation point, all the three ridge pixels in M that are

Copyright ⓒ 2014 SERSC

connected to it are initialized to 3 (Figure 7(d) and the number of transitions from 0 to 3 (T03) (Figure 8(b)) are counted along the border of image M in clockwise direction. If T03 = 3, then the candidate point is validated as a true bifurcation point. The flowchart of the algorithm is presented in Figure 9.

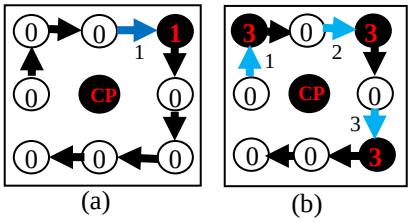

Figure 8. 0 to 1 Transitions. (a) Ridge Ending (T_{01}=1), (b) Bifurcation (T_{03}=3)

4. Experimental Study

The experiments based on Matlab application were carried out using FVC2000, FVC2002 and FVC2004 standard fingerprint databases on Ms-Window 7 Operating System on a Pentium 4 – 2.80 GHz dual processors with 4.00GB of RAM. The summary of the three standard databases is presented in Table 2 [48-49]. The three databases were jointly formulated by the Biometric System Laboratory of the University of Bologna, together with the Biometric Test Centre of the San Jose State University and the Pattern Recognition and Image Processing Laboratory of the Michigan State University. There are four datasets in each of the three databases and each dataset has 80 fingerprints of different qualities and obtained at different resolution, orientation and sizes on the basis of 8 enrolments from each of 10 different people.

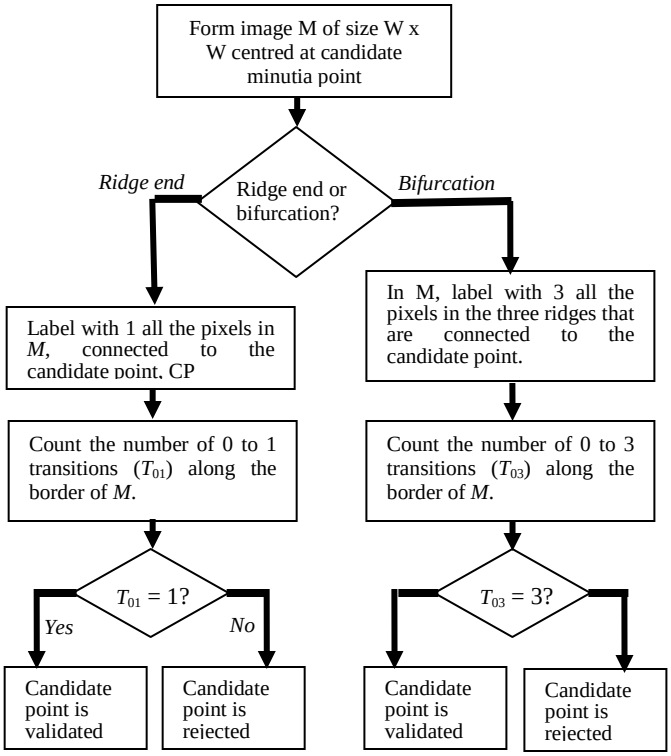

Figure 9. Flowchart for Minutiae Validity Test

Copyright ⓒ 2014 SERSC

Table 2. Details of the Standard Fingerprint Databases

Data-base	Sensor Type			Image size			No.	Resolution		
	FVC2000	FVC2002	FVC2004	FVC2000	FVC2002	FVC2004		FVC2000	FVC2002	FVC2004
DB1	Optical Sensor			300 x 300	388 x 374	640 x 480	100 x 8	500 dpi	500 dpi	500 dpi
DB2	Capacitive Sensor	Optical Sensor		256 x 354	296 x 560	328 x 364	100 x 8	500 dpi	569 dpi	500 dpi
DB3	Optical Sensor	Capacitive Sensor	Thermal Sweeping	448 x 478	300 x 300	300 x 480	100 x 8	500 dpi	500 dpi	512 dpi
DB4	SFinGe v2.0	SFinGe v2.51	SFinGe v3.0	240 x 320	288 x 384	288 x 384	100 x 8	About 500 dpi	About 500 dpi	About 500 dpi

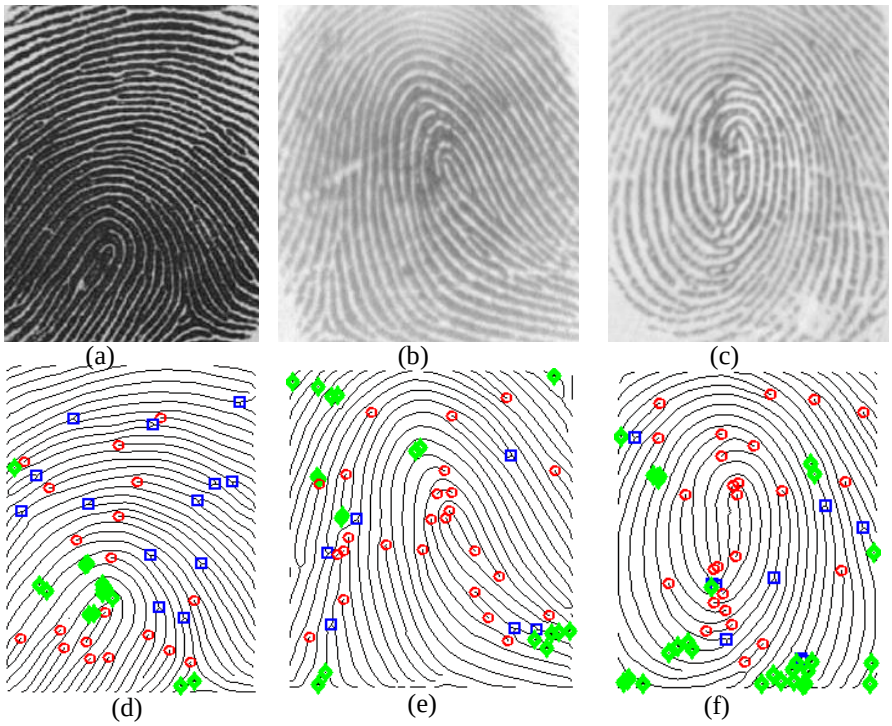

Figure 10. Fingerprint Images from Standard Databases and their True and False Minutiae Points

The detailed results for the pre-processing sub-stages of segmentation, normalization, filtering, binarization and thinning had been discussed in [50] and they are excluded from this report. Formatted images from datasets DB1 of FVC2000, FVC2002 and FVC2004 standard databases are shown in Figure 10 (a), 10(b) and 10(c) respectively. Figures 10(d), 10(e) and 10(f) present the extracted minutiae based on CN algorithm from the skeleton (thinned) images of Figure 10(a), 10(b) and 10(c) respectively.

The true ridge ends points are shown with circles (red color), the square marks (blue color) represent the true bifurcation points and the false minutiae points are denoted with diamonds (in green). The ratio of true to false ridge end points extracted and shown in Figure 10(d), 10(e) and 10(f) are 19:13, 25: 14 and 26: 13 respectively. For bifurcation points, the ratio is 13:7, 6:13 and 9:19 respectively. The results from the minutiae extraction experiments on the three standard fingerprint databases using the CN algorithm are presented in Table 3. Higher values are recorded for false minutiae points over true minutiae points in all cases. As shown

Copyright ⓒ 2014 SERSC

in Figures 11 and 12, there are higher percentages for false ridge end and bifurcation points in all the datasets and databases.

Table 3. Statistics of Extracted True and False Minutiae from the Three Databases

Dataset		FVC2000		FVC2002		FVC2004	
		Total	Time(s)	Total	Time(s)	Total	Time(s)
DB1	Ridge end	10683	91.86	6980	119.01	10822	200.20
	Bifurcation	6254		9545		12389	
DB2	Ridge end	7914	97.05	22425	158.93	14962	114.37
	Bifurcation	8008		14156		11276	
DB3	Ridge end	54165	231.34	13124	91.81	18198	133.95
	Bifurcation	46681		15676		12565	
DB4	Ridge end	6269	73.35	17735	97.95	14544	100.32
	Bifurcation	8147		12873		12137	

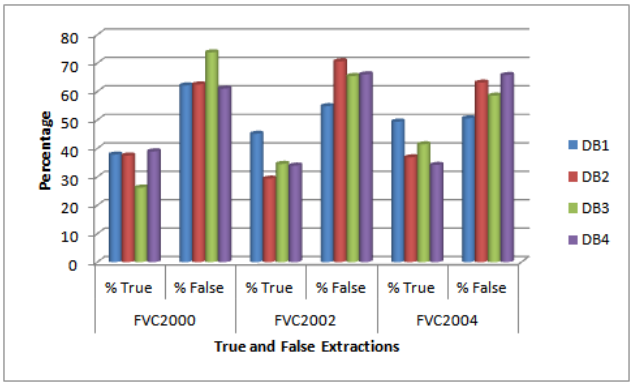

Figure 11. Percentage of True and False Extracted Ridge Ends

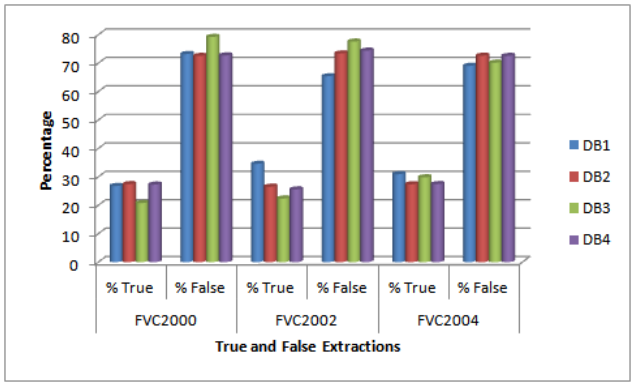

Figure 12. Percentage of True and False Extracted Bifurcations

The exceedingly higher number of extracted false minutiae points is attributed to the presence of high cases of corrupted regions in several of the images. The corrupted regions resulted in the introduction of a great number of artifacts during enhancement [3] some of which appear in form of ridge ends while others as bifurcations. In Figure 13, a highly corrupted image in dataset DB3 of FVC2000 fingerprint database is presented with its extracted true and false minutiae points. It is revealed how the false minutiae points (marked

Copyright ⓒ 2014 SERSC

with 'X') with numerous overlaps, outnumbered the true minutiae points (shown in circles and squares). A total of 123 false minutiae extraction is recorded as against 59 for true minutiae points.

Since different enrolment (from same or different fingers) experience different level of corruption (noise and contaminations), it is therefore consequential that different number of true and false minutiae points will be generated for different images. It also implied that the extraction of different number of false minutiae from images of the same finger will pose a great challenge to reliable implementation of AFIS.

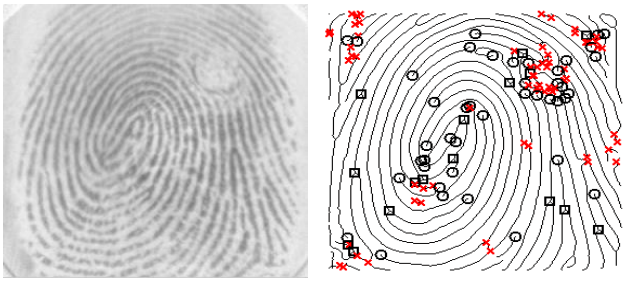

Figure 13. Fingerprint Image and its Extracted True and False Minutiae Points

In the next stage, an implementation of the extension of the CN algorithm with the post-processing algorithm was carried out with a view to eliminating all the false minutiae points. For the purpose of obtaining the best results, the window size, W was experimentally determined. Most appropriate and accurate extraction of true minutiae points as well as rejection of false minutiae points were recorded for W=23 as shown in Figure 14(b). With W < 23, the algorithm was misled into considering some false points as true as shown in Figure 14(a). False rejection of some true points was also experienced with W > 23 as presented in Figure 14(c). With W=23, the results for Figures 10(d), 10(e) and 10(f) are shown in Figure 15(a), 13(b) and 15(c) respectively.

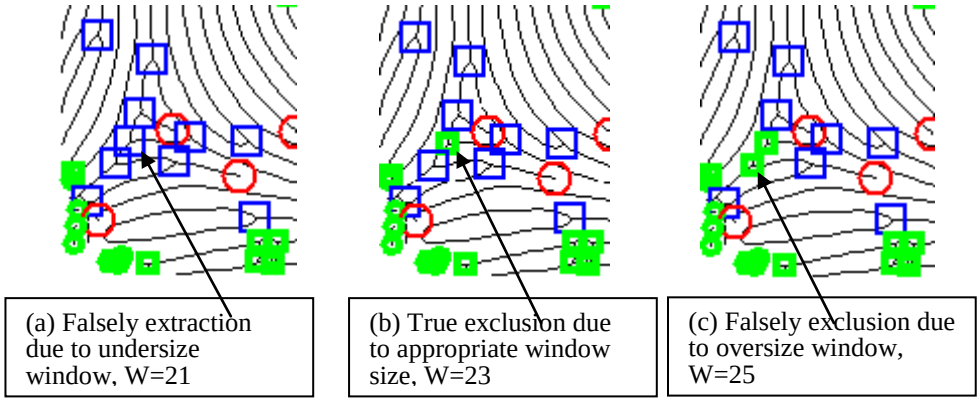

Figure 14. Results Showing the Impact of Window Size of True Minutiae Extraction

The summary of the results of the elimination of all false minutiae points from the images in the three databases are presented in Table 4. The summary shows very significant reduction in the number of extracted minutiae but increase in the completion time when compared with Table 3.

Copyright ⓒ 2014 SERSC

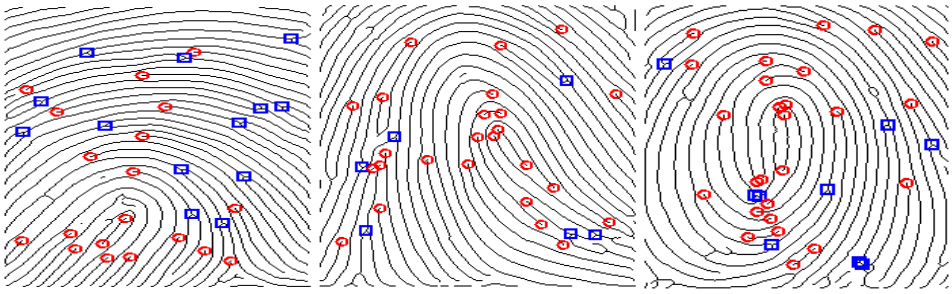

(a)Results of post-processing algorithm for Fig. 10(a)

(b)Results of post-processing algorithm for Fig. 10(b)

(c)Results of post-processing algorithm for Fig. 10(c)

Figure 15. Results Showing the Elimination of False Minutiae Point

Table 4. Results based on Post-Processing Algorithm

Dataset		FVC2000		FVC2002		FVC2004	
		Total	Time(s)	Total	Time(s)	Total	Time(s)
DB1	Ridge end	4042	99.88	3151	129.10	5349	210.17
	Bifurcation	1675		3302		3832	
DB2	Ridge end	2966	104.15	6587	172.08	5515	126.34
	Bifurcation	2197		3759		3088	
DB3	Ridge end	14200	254.38	4532	102.44	7543	143.98
	Bifurcation	9694		3510		3750	
DB4	Ridge end	2442	79.86	6021	109.48	4972	110.89
	Bifurcation	2223		3293		3331	

The increase in the completion time is the time taken to validate or reject each minutia point.

Based on a fingerprint pattern matching algorithm, false rejection and acceptance rates experiments were performed on the three databases for the investigation of the impact of the false minutiae points on fingerprint matching. The algorithm involves the following steps [51]:

a. The core point is extracted based on the algorithm proposed in [52].
b. The equations of the straight lines connecting all the feature points in the 11 x 11 neighbourhood of the core point of an image are calculated. Typical interconnection lines for minutiae points A, B, C, D and E and their intersection points a, b and c are illustrated in Figure 16.

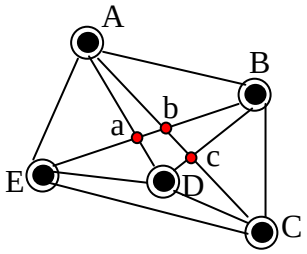

Figure 16. Typical Minutiae Interconnection Lines and their Intersection Points

Copyright ⓒ 2014 SERSC

Given that points $P_1(\rho_1, \tau_1)$ and $P_2(\rho_2, \tau_2)$ are two feature points located in the 11 x 11 neighbourhood of the core point, the equation of the straight line P_1P_2 is given by:

$$y = \varphi x + \partial \tag{11}$$

φ is the gradient of line P_1P_2 and ∂ is defined by:

$$\partial = 0.5((\tau_1 + \tau_2)(\rho_1 - \rho_2) - (\tau_1 - \tau_2)(\rho_1 + \rho_{2\delta})) * (\rho_1 - \rho_2)^{-1} \tag{12}$$

c. The locations of all intersection points in the 11 x 11 neighbourhood of the core (or delta) point are obtained by solving the equations of all intersecting lines. Given that the straight lines AB and CD shown in Figure 17 are defined by equations $\Delta_1 x + \nabla_1 y = \delta$ and $\Delta_2 x + \nabla_2 y = \vartheta$ respectively, then the intersection point J(e,f) is obtained from:

$$e = \left(\delta(\Delta_2\nabla_1 - \Delta_1\nabla_2) - \nabla_1(\Delta_2\delta - \Delta_2\vartheta)\right) * (\Delta_1(\Delta_2\nabla_1 - \Delta_1\nabla_2))^{-1} \tag{13}$$

$$f = (\Delta_2\delta - \Delta_1\vartheta)(\Delta_2\nabla_1 - \Delta_1\nabla_2)^{-1} \tag{14}$$

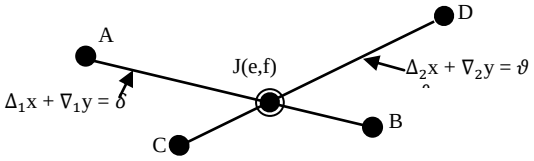

Figure 17. Junction Point of Straight Line Formed by Feature Points

c. The distance, ω_i between the i^{th} intersection point $J_i(e_i,f_i)$ and the image core point $M(\alpha, \beta)$ is obtained from:

$$\omega i = ((e_i - \alpha)^2 + (f_i - \beta)^2)^{0.5} \tag{15}$$

d. For query and reference images with ρ and σ intersection points respectively, the degree of closeness, γ_c is obtained from:

$$\gamma_c = \sum_{i=1}^{n} \frac{|P(i) - I(i)|}{P(i)} \tag{16}$$

$$n = \begin{cases} \rho, & if\ \rho \le \sigma \\ \sigma, & otherwise \end{cases} \tag{17}$$

P(i) and I(i) represent the distance between the i^{th} intersection point and the core point for the query and reference image respectively.

e. The cross-correlation coefficient value for the two images is the pattern matching score, C obtained from:

$$C = 1 - \frac{\gamma_c}{100} \tag{18}$$

The degree of closeness will be γ_c = 0 for exact images and, consequently, the cross-correlation will be C = 1.

The false acceptance experiments measured the rate at which images from different fingers are found to match (matching value exceeding threshold). The false rejection experiments also measured the rate at which images from same finger failed to match (matching value falling below threshold). In all the datasets, matching experiments based on minutiae extracted using CN algorithm (which produced true and false minutiae) in one hand and post-processing algorithm (which produced only true minutiae points) on the other hand, resulted

Copyright ⓒ 2014 SERSC

in False Acceptance Rate (FAR) of 0%. The ROC curves for results based on experiments on false and true minutiae point on the datasets of the 3 fingerprint databases are presented in Figures 18(a-c).

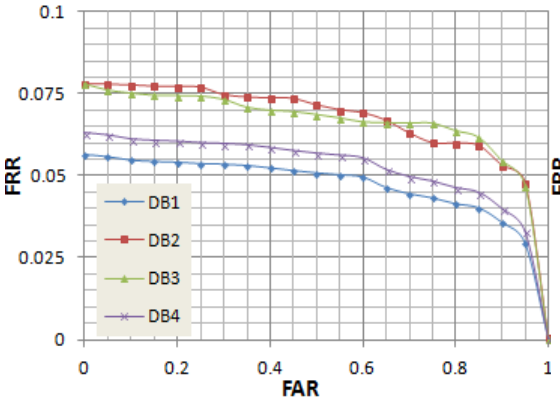

Figure 18. (a) ROC Curve for Matching with True and False Minutiae in FVC2000 Fingerprint Database

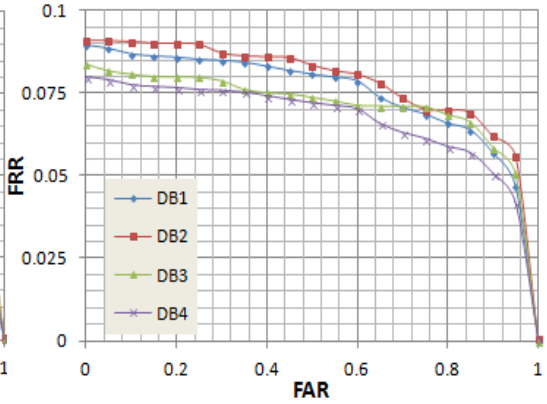

Figure 18. (b) ROC Curve for Matching with True and False Minutiae in FVC2002 Fingerprint

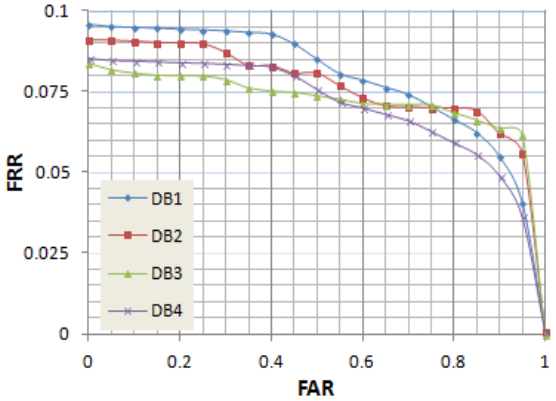

Figure 18. (c) ROC Curve for matching with true and false minutiae in FVC2004 Fingerprint Database

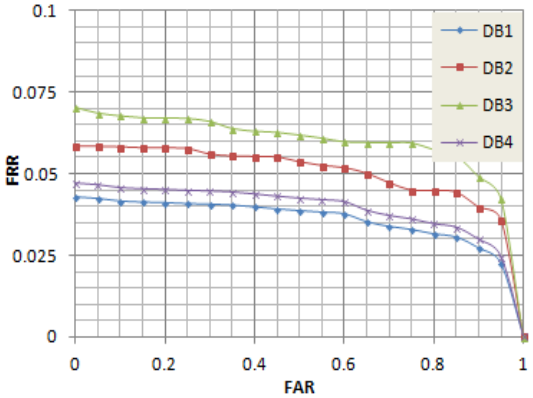

Figure 18. (d) ROC Curve for matching with true minutiae in FVC2000 Fingerprint Database

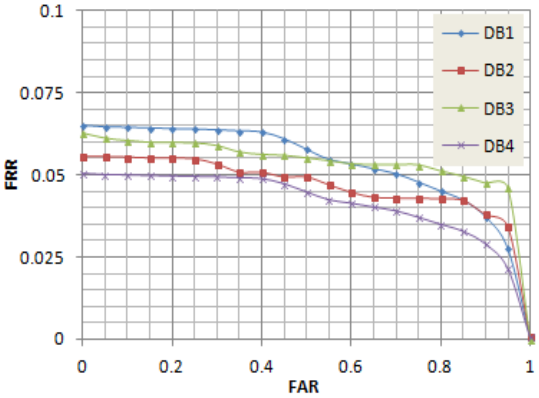

Figure 18. (e) ROC Curve for matching with true minutiae in FVC2002 Fingerprint Database

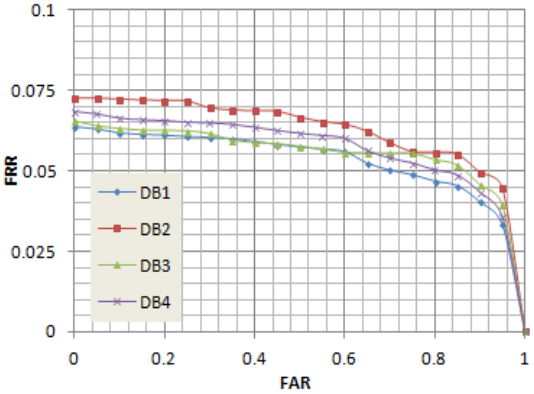

Figure 18. (f) ROC Curve for matching with true minutiae in FVC2004 Fingerprint Database

Copyright ⓒ 2014 SERSC

Figures 18(d-f) present the ROC curves for results from experiments on true minutiae points only. It is revealed from the curves that matching based on true minutiae points only produced lower error rates for all the datasets. This indicates greater accuracy, reliability and efficiency when false points are eliminated from the minutiae set. The higher error rates for matching inclusive of false minutiae points imply that the presence of false minutiae points is capable of worsening the performance of a fingerprint matching algorithm.

The completion times (in seconds) for FAR and FRR experiments on the 80 fingerprint images in each of the datasets for every standard database are shown in Tables 5 and 6. Based on the figures presented, Figures 19 and 20 clearly show very wide gaps between the computation times for FAR and FRR in the CN and post-processing algorithms-based experiments. The lower completion times for the post-processing-based experiments are attributed to lower number of minutiae searches and minimum computations. Statistical analysis of the values presented in Tables 5 and 6 also revealed that matching inclusive of false minutiae points take about 3.5, 3.29 and 2.86 times the time for true minutiae-based matching for all the datasets in FVC2000, FVC2002 and FVC2004 standard databases respectively. It is therefore obvious that the elimination of all false minutiae points at the feature extraction stage in a fingerprint pattern matching system is a necessity for reliable, high speed and user friendly operation.

Table 5. Completion Time (in seconds) for True Minutiae-based Fingerprint Matching

	FVC2000		FVC2002		FVC2004	
	FAR	FRR	FAR	FRR	FAR	FRR
DB1	12.62	11.51	15.33	14.65	13.14	12.36
DB2	14.11	12.37	21.92	18.31	16.70	14.21
DB3	15.90	14.52	22.91	21.33	15.01	15.32
DB4	11.73	13.57	12.34	17.95	12.62	14.94

Table 6. Completion Time (in seconds) for Fingerprint Matching Inclusive of False Minutiae

Dataset	FVC2000		FVC2002		FVC2004	
	FAR	FRR	FAR	FRR	FAR	FRR
DB1	44.17	40.28	50.43	48.19	37.58	35.34
DB2	49.38	43.29	72.11	60.23	47.76	40.64
DB3	55.65	50.82	75.37	70.17	42.92	43.81
DB4	41.05	47.49	40.59	59.05	36.09	42.72

The reliability of the obtained results was further investigated through comparison of its obtained ERR results with those from the implementation of the algorithms proposed in [Bebis *et al.*, [53]; Liu *et al.*, [54]; Liang *et al.*, [55] on FVC2000 with respect to matching accuracy and efficiency. The comparison is presented in Table 7. The EER, which is commonly used to summarize the accuracy performance of a matching system, is defined as the error rate at which the system's FAR and FRR are equal.

Copyright ⓒ 2014 SERSC

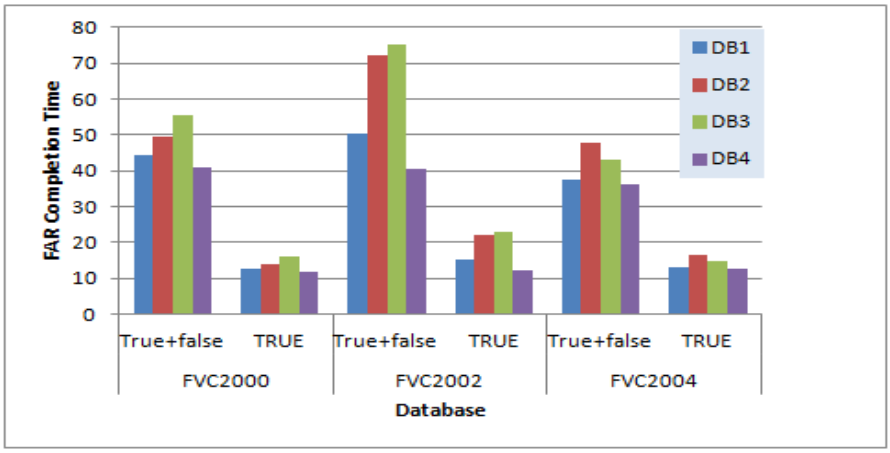

Figure 19. FAR Completion Times

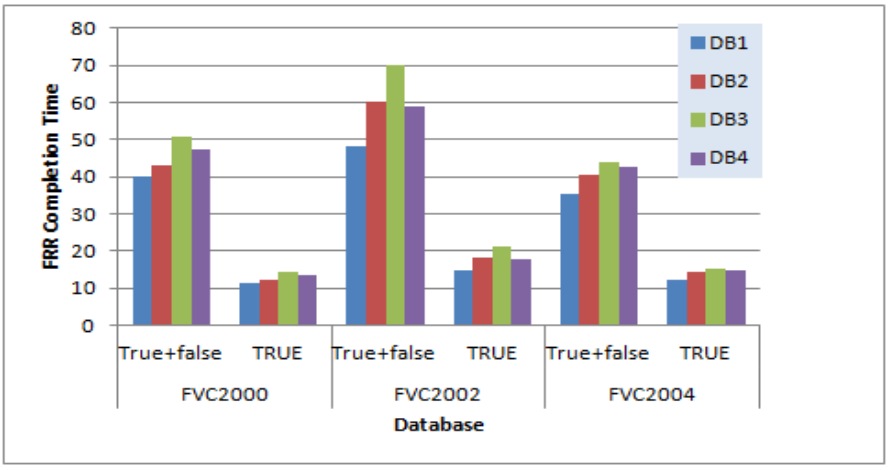

Figure 20. FRR Completion Times

Table 7. ERR (%) Results for Different Algorithms

	DB1	DB2	DB3	DB4
Current study	0.56	0.86	0.95	0.69
Bebis et al. [53]	1.56	2.35	3.05	1.89
Liu et al. [54]	2.78	3.57	4.18	2.94
Liang et al. [55]	0.75	0.98	1.20	0.84

Table 7 shows that, in comparison with the other algorithms, the research fingerprint matching algorithm (RA) is able to achieve matching with the least error results in all the four datasets. The EERs, for example, on DB1 for Bebis *et al.*, [53], Liu *et al.*, [54] and Liang *et al.*, [55] are 0.56%, 1.56%, and 0.75%, respectively as against 0.56% recorded for RA. Further proof of the best performance for RA is presented on the ROC curves in Figure 21 This feat is attributed to the appropriate use of local and neighbourhood feature characteristics in RA.

Copyright ⓒ 2014 SERSC

5. Conclusion

This paper presented a report on the experimental study of the impact of false minutiae points on the performance of AFIS. A 3-tier algorithm was implemented with the results at each level showing relevance and meaningfulness. Results for the first phase of fingerprint minutiae extraction revealed the extraction of true minutiae points. At the post-processing stage, only the true minutiae points; namely ridge end and bifurcation were extracted. Analysis of experimental results for both feature extraction and post-processing algorithms on FVC2000, FVC2002 and FVC2004 fingerprint databases revealed that for speedy and reliable performance of AFIS, all forms of false minutiae points must be eliminated from its operation.

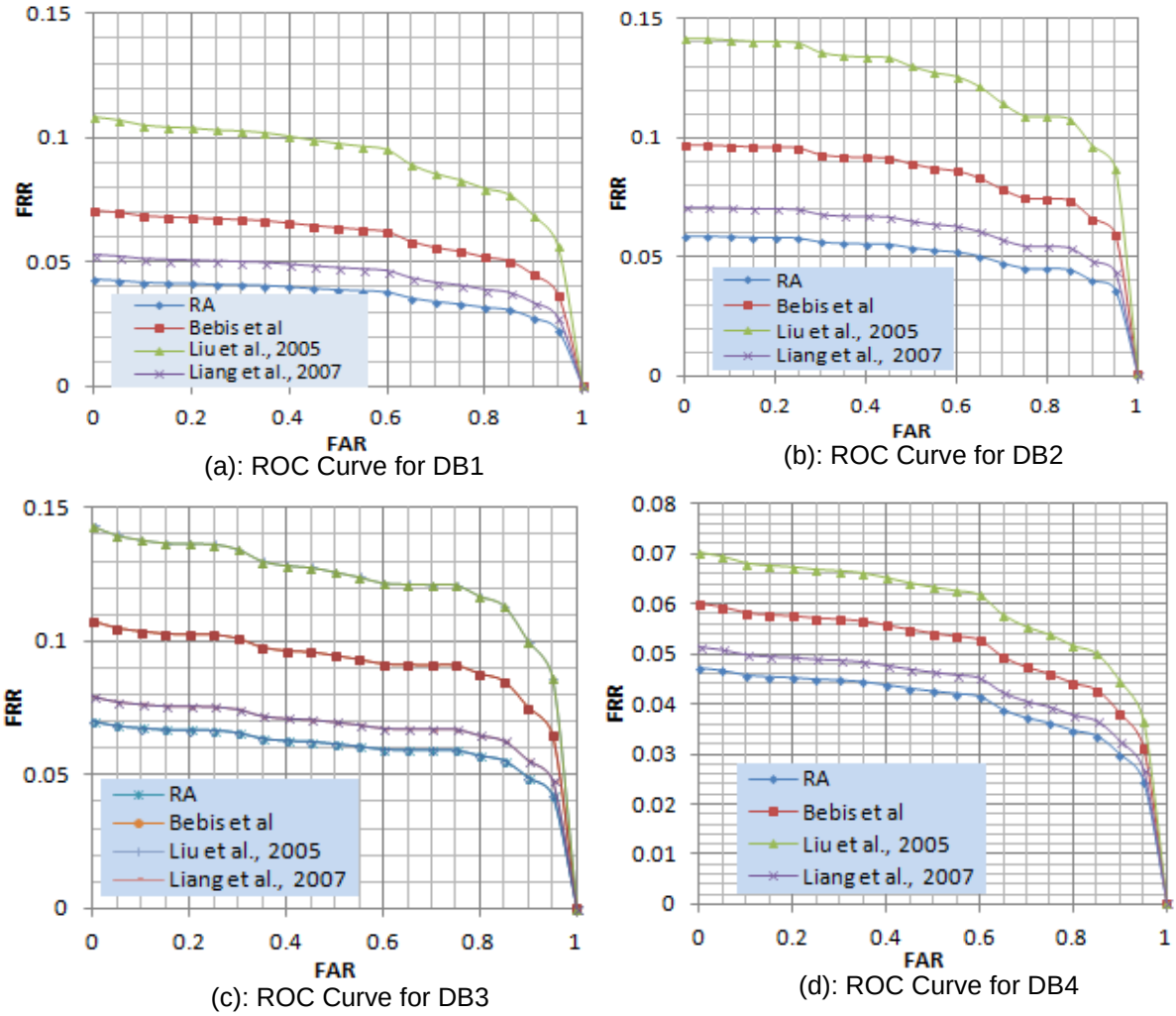

(a): ROC Curve for DB1

(b): ROC Curve for DB2

(c): ROC Curve for DB3

(d): ROC Curve for DB4

Figure 21. ROC Curves for Four Different Algorithms on Datasets of FVC2004 Fingerprint Database

Copyright ⓒ 2014 SERSC

References

[1] C. Robert, R. Milton and D. Morrow, "Automated Fingerprint Identification Systems, Computer world Honours: Case Study", (www.cwhonors.org/archives/case_studies/ Acxiom.pdf). Accessed 12/011/2013, **(2005)**.
[2] Z. Jinhai, L. Xinjian and C. Bo, "The Design and Implementation of ID Authentication System Based on Fingerprint Identification", Proceedings of Fourth International Conference on Intelligent Computation Technology and Automation (kresttechnology.com). Accessed 16/12/2013, **(2011)**.
[3] A. K. Anil, S. Prabhakar and S. Chen, "Combining Multiple Matchers for a High Security Fingerprint Verification System", Pattern Recognition Letters, vol. 20, **(1999)**, pp. 1371-1379.
[4] G. B. Iwasokun, O. C. Akinyokun and O. Olabode, "A Mathematical Modelling Approach to Fingerprint Ridge Segmentation and Normalization", International Journal of Computer Science and Information Technology & Security, Singapore, vol. 2, no. 2, **(2012)**, pp. 263-267.
[5] S. Pannirselvam and P. Raajan, "An Efficient Fingerprint Enhancement Filtering Technique with High Boost Gaussian Filter (HBG)", International Journal of Advanced Research in Computer Science and Software Engineering, vol. 2, no. 11, **(2012)**.
[6] L. Hong, Y. Wan and A. Jain, "Fingerprint Image Enhancement: Algorithm and Performance Evaluation", IEEE Transactions on Pattern Analysis and Machine Intelligence, vol. 20, **(1998)**, pp. 777–789.
[7] Y. Jianwei, L. Liu, T. Jiang and Y. Fan, "A Modified Gabor Filter Design Method for Fingerprint Image Enhancement", Pattern Recognition Letters, vol. 24, **(2003)**, pp. 1805–1817.
[8] K. Hongchang, H. Wang and D. Kong, "An Improved Gabor Filtering for Fingerprint Image Enhancement Technology", Proceedings of the 2nd International Conference on Electronic & Mechanical Engineering and Information Technology (EMEIT-2012).
[9] R. Dhanabal, V. Bharathi, G. P. Jain , G. Hariharan, P. D. Ramkumar and S. K. Sahoo, "Gabor Filter Design for Fingerprint Application Using Matlab and Verilog HDL", International Journal of Engineering and Technology (IJET), vol. 5, no. 2, **(2013)**, pp. 1386-1391.
[10] M. P. Mudegaonkar and R. P. Adgaonkar, "A Novel Approach to Fingerprint Identification Using Gabor Filter-Bank", ACEEE International Journal on Network Security, vol. 2, no. 3, **(2011).**
[11] S. Chikkerur, V. Govindaraju and N. Alexander, "Fingerprint Image Enhancement Using STFT Analysis", S. Singh et al. (Eds.): ICAPR 2005, LNCS 3687, **(2005)**, pp. 20–29.
[12] B. G. Sherlock, D. M. Monro and K. Millard, "Fingerprint Enhancement by Directional Fourier Filtering", IEE Proc. Vision Image Signal Process, vol. 141, no. 2, **(1994)**, pp. 87–94.
[13] V. R. Aarthy, M. Mythili and M. Mahendran, "Low Quality Fingerprint Image Using Spatial and Frequency Domain", International Journal of Computational Engineering Research, vol. 2, no. 6, **(2012)**.
[14] J. S. Bartunek, M. Nilsson, J. Nordberg and I. Claesson, "Adaptive Fingerprint Binarization by Frequency Domain Analysis", http://www.bth.se/fou/forskinfo.nsf/all /bb66330d02d2801cc125733e008178d6/ $file/Paper.pdf, Accessed 12/02/2013, **(2006)**.
[15] G. B. Iwasokun, O. C. Akinyokun, B. K. Alese and O. Olabode, "Adaptive and Faster Approach to Fingerprint Minutiae Extraction and Validation", International Journal of Computer Science and Security, Malaysia, vol. 5, no. 4, **(2011)**, pp. 414-424.
[16] B. V. Bhalerao and R. R. Manza, "Development of Image Enhancement and the Feature Extraction Techniques on Rural Fingerprint Images to Improve the Recognition and the Authentication Rate", IOSR Journal of Computer Engineering (IOSR-JCE), (www.iosrjournals.org www.iosrjournals.org), vol. 15, no. 1, **(2013)**, pp. 01-05.
[17] N. K. Ratha, S. Chen and A. K. Jain, "Adaptive Flow Orientation-based Feature Extraction in Fingerprint Images", Pattern Recognition, vol. 28, no. 11, **(1995)**, pp. 1657-1672.
[18] K. R. Moses, P. Higgins, M. McCabe, S. Prabhakar and S. Swann, "Automated Fingerprint Identification System (AFIS)", (https://www.ncjrs.gov/pdffiles1/nij/ 225326.pdf). Accessed 01/11/2013.
[19] N. Ratha, S. Chen and A. K. Jain, "Adaptive Flow Orientation Based Feature Extraction in Fingerprint Images", Pattern Recognition, vol. 28, no. 11, **(1995)**, pp. 1657-1672.
[20] S. Kasaei, M. Deriche and B. Boashash, "Fingerprint Feature Enhancement using Block Direction on Reconstructed Image", (Unpublished) (sina.sharif.edu/~skasaei/Papers/ icics02.pdf). Accessed 07/02/2014.
[21] V. Humbe, S. S. Gornale, R. Manza and K. V. Kale, International Journal of Computer Science and Security, vol. 1, no. 2, **(2007)**.
[22] G. Shevaani and S. Thapar, "Feature extraction using Morphological Operations on Fingerprint Images", International Journal of Computing and Business Research, (www.researchmanuscripts.com/isociety2012/40.pdf). Accessed 12/01/2014, **(2012)**.
[23] F. Alessandro, Z. M. Kovacs-Vajna and A. Leone, "Fingerprint Minutiae Extraction from Skeletonised Binary Images", Pattern Recognition, vol. 32, **(1999)**.

 Copyright ⓒ 2014 SERSC

[24] D. Arpit and A. Namboodiri, "Fingerprint Feature Extraction from Gray Scale Images by Ridge Tracing", http://www.csis.pace.edu/~ctappert/dps/2011IJCB/papers/200.pdf, Accessed 16/05/2013, **(2011)**.
[25] S. Kamil, K. Saeed and P. Rapta, "An Improved Algorithm for Feature Extraction from a Fingerprint Fuzzy Image", Optica Applicata, vol. XLIII, no. 3, **(2011)**.
[26] H. Fronthaler, K. Kollreider and J. Bigun, "Local Feature Extraction in Fingerprints by Complex Filtering", S.Z. Li et al. (Eds.): IWBRS 2005, LNCS 3781, Springer-Verlag Berlin Heidelberg, **(2005)**, pp. 77–84.
[27] L. Chih-Jen and W. Sheng-De, "Fingerprint Feature Extraction Using Gabor Filters", Electronic Letters, vol. 35, no. 4, **(1999)**.
[28] C. Jianping and H. Tiejun, "A Robust Feature Extraction Algorithm for Audio Fingerprinting", (http://159.226.42.3/doc/2008/A%Robust A%Feature A%Extraction A%Algorithm A%for A%Audio A%Fingerprinting.pdf). Accessed 09/02/2014, **(2008)**.
[29] R. Choonwoo, S. G. Kong and H. Kim, "Enhancement of Feature Extraction for Low-quality Fingerprint Images Using Stochastic Resonance", Pattern Recognition Letters, vol. 32, **(2011)**, pp. 107-113.
[30] G. Qun and G. S. Moschytz, "Fingerprint Feature Extraction Using CNNs", Proceedings of European Conference on Circuit Theory and Design, Espoo, Finland, **(2001)** August 28-31.
[31] D. C. Lakshmi, A Kandaswamy, C. Vimal and B. Sathish, "Invariant Feature Extraction from Fingerprint Biometric Using Pseudo Zernike Moments", Singaporean Journal Scientific Research (SJSR), http://www.iaaet.org/sjsr, vol. 3, no. 2, **(2010)**, pp. 150-154.
[32] A. I. Awad, "Fingerprint Local Invariant Feature Extraction on GPU with CUDA", Informatica, vol. 37, **(2013)**, pp. 279–284.
[33] Y. Jianwei, L. Liu and T. Jiang, "An Improved Method for Extraction of Fingerprint Features", (nlpr-web.ia.ac.cn/English/mic/jianweiyang/ICIG_yang.pdf), Accessed 10/02/2014, **(2001)**.
[34] N. J. Short, "Robust Feature Extraction and Temporal Analysis for Partial Fingerprint Identification", PhD Thesis (unpublished) submitted to the Faculty of the Virginia Polytechnic Institute and State University, **(2012)**.
[35] L. Chih-Jen and W. Sheng-De, "Fingerprint Feature Extraction Using Gabor Filters", Electronic Letters, vol. 35, no. 4, **(1999)**.
[36] M. Awasthi and A. Sharma, "An Efficient Algorithm for Minutia Feature Extraction Method", VSRD International Journal of Electrical, Electronic and Communication Engineering, vol. 2, no. 8, **(2012)**, pp. 585-593.
[37] M. R. Teague, "Image Analysis via the general theory of moments", Journal of Optical Society, vol. 23, **(1975)**.
[38] C. H. The and R. T. Chin, "On Image Analysis by the Methods of Moments", IEEE Transactions on Pattern Analysis Machine Intelligent, vol. 10, no. 4, **(1988)**, pp. 496- 513.
[39] S. Mirarab, A. Hassouna and L. Tahvildari, "Using Bayesian Belief Networks to Predict Change Propagation in Software Systems", Proceeding of IEEE 15th International Conference on Program Comprehension (ICPC '07), **(2007)**, pp. 177-188.
[40] H. Liu, W. Yifei and J. K. Anil, "Fingerprint Image Enhancement: Algorithm and Performance Evaluation", Pattern Recognition and Image Processing Laboratory, Department of Computer Science, Michigan State University, **(2006)**, pp. 1-30.
[41] R. Thai, "Fingerprint Image Enhancement and Minutiae Extraction", PhD Thesis (Unpublished) Submitted to School of Computer Science and Software Engineering, University of Western Australia, **(2003)**, pp. 21-56.
[42] G. B. Iwasokun, O. C. Akinyokun and O. Olabode, "A Block Processing Approach to Fingerprint Ridge Orientation Estimation", Journal of Computer Technology and Application, USA, vol. 3, **(2012)**, pp. 401-407.
[43] V. C. Arun, "Extracting and Enhancing the Core Area in Fingerprint Images", IJCSNS International Journal of Computer Science and Network Security, vol. 7, no. 11, **(2007)**, pp. 16-20.
[44] G. B. Iwasokun, O. C. Akinyokun and O. Olabode, "Uniformity Level Approach to Fingerprint Ridge Frequency Estimation", International Journal of Computer Applications, USA, vol. 61, no. 22, **(2013)**, pp. 26-32.
[45] L. Xu, "Image Binarization using Otsu Method", Proceedings of NLPR-PAL Group CASIA Conference, **(2009)**, pp. 345-349.
[46] S. S. Ponnarasi and M. Rajaram, "Impact of Algorithms for the Extraction of Minutiae Points in Fingerprint Biometric", Journal of Computer Science, vol. 8, no. 9, **(2012)**, pp. 1467-1472.
[47] Q. Xiao and H. Raafat, "Fingerprint image Post-processing: A Combined Statistical and Structural Approach", Pattern Recognition, vol. 24, no. 10, **(1991)**, pp. 985–992.
[48] R. Cappelli, D. Maio, D. Maltoni, J. L. Wayman and A. K. Jain, "Performance Evaluation of Fingerprint Verification Systems", IEEE Transactions on Pattern Analysis and Machine Intelligence, vol. 28, no. 1, **(2006)**, pp. 3-18.

Copyright ⓒ 2014 SERSC

[49] J. Cheng and J. Tian, "Fingerprint Enhancement with Dyadic Scale-Space", Pattern Recognition Letters, Elsevier B.V, **(2004)**.
[50] G. B. Iwasokun, O. C. Akinyokun, C. O. Angaye and O. Olabode, "A Multi-Level Model for Fingerprint Enhancement", Journal of Pattern Recognition Research, USA, vol. 7, **(2012)**, pp. 155-174.
[51] G. B. Iwasokun, O. C. Akinyokun and C. O. Angaye, "Fingerprint Matching using Neighbourhood Distinctiveness", International Journal of Computer Applications, USA, vol. 66, no. 21, **(2013)**.
[52] S. Basak, I. Islam and M. R. Amin, "Detection of Virtual Core Point of A Fingerprint: A New Approach", International Journal of Soft Computing and Engineering (IJSCE), vol. 2, no. 2, **(2012)**.
[53] G. Bebis, T. Deaconu and M. Georgiopoulos, "Fingerprint Identification Using Delaunay Triangulation", http://www.cse.unr.edu/~bebis/CS790Q/ PaperPresentations/fingerprintICIIS99.pdf, Accessed 06/05/2013.
[54] N. Liu, Y. Yin and H. Zhang, "A Fingerprint Matching Algorithm Based On Delaunay Triangulation Net", Proceedings of Fifth International Conference on Computer and Information Technology (CIT'05), **(2005)**.
[55] X. Liang, T. Asano and A. Bishnu, "Distorted Fingerprint Indexing Using Minutia Detail and Delaunay Triangle", www.jaist.ac.jp/jinzai/Paper18/ISVD2006.pdf, Accessed 23/04/2013.

 Copyright ⓒ 2014 SERSC